Development/Plasticity/Repair

Reduced $GABA_A$ Receptor-Mediated Tonic Inhibition in Aged Rat Auditory Thalamus

Ben D. Richardson,[1] Lynne L. Ling,[1] Victor V. Uteshev,[1,2] and Donald M. Caspary[1]

[1]Department of Pharmacology, School of Medicine, Southern Illinois University, Springfield, Illinois 62794, and [2]Department of Pharmacology and Neuroscience, University of North Texas Health Science Center, Fort Worth, Texas 76107

Age-related deficits in detecting and understanding speech, which can lead to social withdrawal and isolation, have been linked to changes in the central auditory system. Many of these central age-related changes involve altered mechanisms of inhibitory neurotransmission, essential for accurate and reliable auditory processing. In sensory thalamus, GABA mediates fast (phasic) inhibition via synaptic $GABA_A$ receptors ($GABA_A$Rs) and long-lasting (tonic) inhibition via high-affinity (extrasynaptic) $GABA_A$Rs, which provide a majority of the overall inhibitory tone in sensory thalamus. Due to a delicate balance between excitation and inhibition, alteration of normal thalamic inhibitory function with age and a reduction of tonic $GABA_A$R-mediated inhibition may disrupt normal adult auditory processing, sensory gating, thalamocortical rhythmicity, and slow-wave sleep. The present study examines age-related homeostatic plasticity of $GABA_A$R function in auditory thalamus or the medial geniculate body (MGB). Using thalamic slices from young adult (3–8 months) and aged (28–32 months) rats, these studies found a 45.5% reduction in $GABA_A$R density and a 50.4% reduction in $GABA_A$R-mediated tonic whole cell Cl^- currents in the aged MGB. Synaptic $GABA_A$R-mediated inhibition appeared differentially affected in aged lemniscal and nonlemniscal MGB. Except for resting membrane potential, basic properties were unaltered with age, including neuronal Cl^- homeostasis determined using the gramicidin perforated patch-clamp method. Results demonstrate selective significant age-dependent deficits in the tonic inhibitory tone within the MGB. These data suggest that selective $GABA_A$R subtype agonists or modulators might be used to augment MGB inhibitory neurotransmission, improving speech understanding, sensory gating, and slow-wave sleep for a subset of elderly individuals.

Introduction

One-third to one-half of individuals over the age of 65 suffer from age-related hearing loss or presbycusis, significantly impairing their quality of life (Cruickshanks et al., 1998; Gordon-Salant et al., 2010). Evident in humans and animal models, impaired performance in temporal discrimination/speech processing tasks, novelty detection, and the ability to attend to acoustic stimuli occur even in the face of large variations in peripheral hair cell and/or spiral ganglion cell losses, suggesting a compromised central auditory system with age (Takahashi and Bacon, 1992; Gordon-Salant and Fitzgibbons, 1993; Snell, 1997; Alain and Woods, 1999; Lister et al., 2002; Tremblay et al., 2003; Caspary et al., 2008; de Villers-Sidani et al., 2010; Gordon-Salant et al., 2010; Humes et al., 2010; Juarez-Salinas et al., 2010; Walton, 2010; Suta et al., 2011; Anderson et al., 2012). One major central component, maladaptive plastic changes in glycinergic and GABAergic inhibitory neurotransmitter markers, is present throughout the central auditory system (Caspary et al., 2008). Age-related changes in inhibitory neurotransmitter systems may have profound functional consequences, as coding of acoustic information by central auditory neurons is dependent on inhibitory neurotransmission (Palombi and Caspary, 1992; Chen and Jen, 2000; Caspary et al., 2002, 2008; Yu et al., 2009).

The medial geniculate body (MGB) is essential for relaying, processing, filtering, and attending to acoustic information, often described as the "gate" to auditory cortex (Edeline, 2011). The three divisions of the MGB [lemniscal ventral (MGv) and nonlemniscal dorsal (MGd) and medial (MGm)] receive glutamatergic input from the inferior colliculus (IC) and auditory cortex, and inhibitory input from the IC, thalamic reticular nucleus (TRN), and a small (~1%) population of interneurons (Winer and Larue, 1996; Winer et al., 1996; Peruzzi et al., 1997; Bartlett and Smith, 1999; Kimura et al., 2007; Edeline, 2011). Currently, GABAergic inhibitory inputs are known to regulate the output of the MGB by shaping frequency response areas and thresholds of MGB neurons (Suga et al., 1997; Cotillon-Williams et al., 2008).

Ionotropic receptor targets of inhibitory GABAergic inputs in MGB are both synaptic $GABA_A$ receptors ($GABA_A$Rs) and high-affinity (extrasynaptic) $GABA_A$Rs, also present in visual and somatosensory thalamus (Wisden et al., 1992; Bartlett and Smith, 1999; Pirker et al., 2000; Belelli et al., 2005; Cope et al., 2005; Jia et al., 2005; Edeline, 2011; Richardson et al., 2011). Synaptic

Received July 10, 2012; revised Nov. 30, 2012; accepted Dec. 3, 2012.

Author contributions: B.D.R., L.L.L., V.V.U., and D.M.C. designed research; B.D.R. and L.L.L. performed research; B.D.R. and L.L.L. analyzed data; B.D.R., L.L.L., V.V.U., and D.M.C. wrote the paper.

This work was supported by National Institutes of Health Grant DC000151. We thank Dr. Pete Hutson for his help and support, Merck (Rahway, NJ) for supplying the [^{3}H]gaboxadol, Dr. Bjarke Ebert of H. Lundbeck A/S (Copenhagen, DK) for his advice, Emily Tignor for her tracing of filled neurons, and Drs. L. Premkumar, E. Sametskiy, B. I. Kalappa, J. L. Parrish, and M. D. Richardson for their input and critique of this manuscript.

The authors declare no competing financial interests.

Correspondence should be addressed to Donald M. Caspary, P.O. Box 19629, Springfield, IL 62794. E-mail: dcaspary@siumed.edu.

DOI:10.1523/JNEUROSCI.3277-12.2013

 0270-6474/13/331218-10$15.00/0

$GABA_AR$s contain α_{1-4}, β_2, and γ_2 subunits, which mediate phasic/fast Cl^- currents, whereas high-affinity $GABA_AR$s containing a δ subunit, exclusively colocalized with the α_4 subunit in the thalamus, forming a second class of $GABA_AR$ constructs that mediate tonic/long-lasting Cl^- currents/inhibition with high agonist affinity and slower desensitization (Sur et al., 1999; Pirker et al., 2000; Sieghart and Sperk, 2002; Chandra et al., 2006; Walker and Semyanov, 2008; Belelli et al., 2009; Herd et al., 2009; Mortensen et al., 2010).

Receptor binding, immunohistochemistry, and whole-cell and gramicidin-perforated patch recordings were performed using young adult (3–8 months) and aged (28–32 months) Fischer Brown Norway (FBN) rats to address the hypothesis that phasic and tonic inhibition in the MGB may be reduced or altered with age.

Materials and Methods

Subjects. Naive young adult (3–8 months) and aged (28–32 months) male FBN rats, a model of age-related presbycusis (Lipman et al., 1996; Caspary et al., 2005; Wang et al., 2009), were used as subjects in all experiments and housed with a 12 h reversed light/dark cycle with *ad libitum* access to food and water. Some methods have been described previously in detail and are described here briefly (Richardson et al., 2011). All procedures were in accordance with the Southern Illinois University School of Medicine Lab Animal Care and Use Committee guidelines and approved protocols.

Western blot. Nine young adult and nine aged FBN rats were decapitated in pairs, and brains were immersed into ice-cold PBS, pH 7.4. The MGB was then dissected and homogenized in TEVP buffer [containing (in mM) 10 Tris base, 5 NaF, 1 Na_3VO_4, 1 EDTA, and 1 EGTA, pH 7.4] with 320 mM sucrose and protease inhibitor (1:100) added to the mixture before homogenization. Homogenates were centrifuged for 10 min at 800 × *g* and collected supernatants at 10,000 × *g* for 15 min, all at 4°C. This supernatant contained the cytosolic fraction. Total protein concentrations were measured using the NanoDrop Analyzer (NanoDrop Products).

Protein samples extracted from the MGB were solubilized by the addition of Laemmli buffer (5×; Sigma-Aldrich) and incubated in boiling water for 8 min. Discontinuous electrophoresis was performed using a stacking gel containing 4% acrylamide and separating gel containing 10% acrylamide. After electrophoresis separation, proteins were transferred to PVDF membranes. Resulting blots were blocked with 1.5% normal serum and 1× blocking reagent (Fisher Scientific) in Tris-buffered saline (TBS), pH 7.4, for 1 h at room temperature, and then incubated with monoclonal mouse anti-GAD_{67} antibody (1:250; Millipore) diluted in blocking solution overnight at 4°C on shaker. After washing, PVDF membranes were incubated with secondary antibody goat anti-mouse IgG-HRP (1:10,000; Santa Cruz Biotechnology) for 1 h at room temperature. Following washes with TBS plus 0.01% Tween 20 (three times, 10 min each) and TBS (5 min), the blots were detected with Western Blotting Luminol Reagent (Santa Cruz Biotechnology) using a Fujifilm LAS-4000 Luminescent Image Analyzer. Multi Gauge software was used to quantify protein bands. β-actin was used as the loading control. Values are expressed as corrected ratios based on the measurement of β-actin. Protein band density from aged samples was expressed normalized to the paired young adult sample run simultaneously (relative protein density = target protein density/β-actin density/paired young adult target protein density).

Confocal fluorescent imaging. Two young adult and two aged FBN rats were anesthetized with a ketamine (105 mg/kg; Aveco) and xylazine (7 mg/kg; Lloyd Laboratories) mixture intramuscularly followed by transcardial perfusion with 100 ml of saline and 750 ml of fixative containing 4% paraformaldehyde in PBS, pH 7.4. Coronal sections (30 μm) were cut through the MGB and collected in PBS. Free-floating sections were processed in parallel and incubated for 30 min in blocking solution containing PBS with 1.5% of normal serum and 3% bovine serum albumin. Sections were then transferred to primary antibody solution [monoclonal mouse anti-GAD_{67} antibody (1:250; Millipore) or goat anti-$GABA_AR$ α_4 and/or rabbit anti-$GABA_AR$ δ (1:100; Santa Cruz Biotechnology)] and incubated for 1 h at room temperature and then overnight at 4°C on shaker. After washing with PBS, sections were incubated with donkey anti-mouse IgG (Dylight 488; 1:100), donkey anti-goat IgG (Dylight 488; 1:100), and donkey anti-rabbit IgG (Rhodamine Red-X; 1:100; Jackson ImmunoReseach) for 1 h at room temperature. As a negative control, the primary antibody was omitted, and no immunolabeling was observed. Neuronal nuclei were counterstained with the diamidino-2-phenylindole (DAPI; Vector Laboratories). Following PBS washing, the sections were mounted onto slides and coverslipped with VectorShield (Vector Laboratories). Fluorescent imaging was performed using a Leica TCS SP5 II confocal laser microscope under identical settings (laser intensity, photomultiplier tube, scanning speed, etc.) for young adult and aged tissues.

Radioligand binding. Binding protocols were identical to those used previously (Richardson et al., 2011). Five young and four aged FBN rats were decapitated, and the brains were rapidly removed, rinsed in ice-cold phosphate buffer at 4°C, pH 7.4, frozen in powdered dry ice, and stored at −80°C. Serial transverse sections were cut at 16 μm using a Leica CM1850 cryostat at −18°C. Selected sections were thaw-mounted onto Superfrost/Plus slides and stored at −20°C. Anatomical locations of the MGB were verified to match neural structures with those described previously (Paxinos and Watson, 1998).

[^{3}H]gaboxadol (a gift from Merck, Inc.) was used with modified protocols from Milbrandt and Caspary (1995) and Dr. Bjarke Ebert (H. Lundbeck A/S, Copenhagen, DK; personal communication). Tissue sections were subjected to prewash twice for 5 min in buffer, followed by incubation with [^{3}H]gaboxadol: 10–400 nM and postwash with buffer for four quick dips. The buffer solution used was 50 mM Tris-citrate, pH 7.1. Nonspecific binding was determined in adjacent sections by the addition of cold excessive GABA to the ligand buffer and was subtracted from total binding.

Dried slides were opposed to [^{3}H]-hypersensitive phosphor screens for 2 d at room temperature. The phosphor screens were scanned using a Cyclone Storage Phosphor System (PerkinElmer). The MGB was outlined and analyzed using OptiQuant Image Analysis software (Canberra Packard), which provided tools for grayscale quantification in digital light units. Digital light units were then converted to nanocuries per milligram protein using a standard curve generated from coexposed [^{3}H]-embedded plastic standards (American Radiolabeled Chemicals). Values from the left and right MGB were averaged for each animal and treated as a single individual sample.

Thalamic brain slice preparation. FBN rats anesthetized with 2.5–3.0% isolfurane gas were decapitated. The brains were rapidly removed and placed in ice-cold solution containing the following (in mM): 250 sucrose, 2.5 KCl, 26 $NaHCO_3$, 1.26 NaH_2PO_4, 5 $MgCl_2$, 0.5 $CaCl_2$, 100 glucose, and 2 kynurenic acid, bubbled with 95% O_2 and 5% CO_2. Horizontal 200–300 μm slices containing the MGB were prepared using a Leica VT 1000P vibratome at 3°C. Slices were perfused for 30 min at 30°C with artificial CSF [ACSF; containing (in mM) 125 NaCl, 3 KCl, 1.26 NaH_2PO_4, 2 $CaCl_2$, 1 $MgCl_2$, 26 $NaHCO_3$, and 10 glucose] and then allowed to equilibrate to room temperature for 30 min before being transferred to the recording chamber individually as needed.

Electrophysiology. Neurons residing in thalamic slices containing the MGd and MGv were visualized using an upright Olympus BX51WI microscope through a 40× objective with infrared DIC Nomarski optics (see Fig. 7*F*). Voltage- and current-clamp recordings were obtained using a MultiClamp-700B amplifier (Molecular Devices). Data were digitized by a Digidata 1440A (Molecular Devices) at 5–20 kHz and filtered at 2–2.5 kHz.

Whole-cell recording pipettes (3–6 MΩ) used in voltage-clamp recordings were filled with an intracellular solution containing (in mM) 140 CsCl, 2 $MgCl_2$, 4 Mg-ATP, 0.3 Na-GTP, 10 Na-HEPES, and 0.1 EGTA, with a pH of 7.25 adjusted with HCl (osmolarity, ~280 mOsm), resulting in a Cl^- equilibrium potential (E_{Cl^-}) value near 0 mV. Pipettes (4–6 MΩ) used for recordings in current-clamp experiments were filled with an internal solution containing the following (in mM): 140 K-gluconate, 1 NaCl, 1.5 $MgCl_2$, 10 HEPES, 2 Mg-ATP, and 0.3 Na-GTP, pH adjusted to 7.35 with KOH (osmolarity, ~270 mOsm). Reported voltage values

obtained with the K-gluconate-based solution are corrected for a 15 mV liquid junction potential (LJP). Intracellular solutions typically contained 0.5% Neurobiotin, and filled cells were traced with a Neurolucida system (MicroBrightField).

Following the formation of a gigaseal (>2 GΩ seal), the membrane was ruptured after 5 min of maintaining a stable cell attached configuration (except when using the K- gluconate-based solution), allowing internal solution present extracellularly to diffuse away. Membrane rupture was monitored and recorded to obtain an approximation of the cell's resting membrane potential, and a 100–300 pA hyperpolarizing current injection was applied for 1–2 s to determine the presence of T-type Ca^{2+} channel bursts (see Fig. 4*C*,*D*). Exclusion criteria included (1) a resting membrane potential below −50 mV or spontaneously active cells having an action potential (AP) amplitude >70 mV, (2) removal of the hyperpolarizing current injection resulting in a multispike burst, and (3) resting membrane input resistance >150 MΩ.

Series resistance, cellular input resistance, and whole-cell capacitance were determined by the application of a 10 mV hyperpolarizing pulse. Cellular input resistance was also determined using the slope of the current–voltage (*I–V*) plot between −65 and −70 mV. In all cases, series resistance was not compensated, and all recordings were conducted at room temperature (~22°C). Recordings that exhibited a series resistance >30 MΩ were discarded.

For perforated patch-clamp recordings, gramicidin (Sigma-Aldrich) was diluted in dimethylsulfoxide to a stock solution concentration of 20 mg/ml. The stock solution was diluted to 100 μg/ml in an intracellular solution containing (in mM) 140 KCl and 10 HEPES, with pH 7.36, adjusted with KOH. The KCl-gramicidin solution was sonicated for 1–3 min at the beginning of each day and sonicated again for 15–30 s before filling the recording pipettes. Each pipette tip was backfilled with gramicidin-free KCl, and the remainder of the pipette was backfilled with KCl-gramicidin. KCl-gramicidin pipettes had a tip resistance of 3.9–4.5 MΩ and a calculated E_{Cl^-} of −2.4 mV. After forming a high-resistance seal (0.8–5.5 GΩ; 2.16 ± 0.38 GΩ), the patch was voltage clamped at −70 mV for 27–72 min (48 ± 5 min), during which time the series resistance steadily decreased, stabilizing at 20.8–43.1 MΩ (29.1 ± 2.1 MΩ). Similar to the methods described previously, from a holding potential of −100 mV, +10 mV steps were applied while a 20 ms application of 1 mM gaboxadol was focally applied to determine the reversal potential for the $GABA_A$R-mediated current or the E_{Cl^-}, regardless of subunit configuration (Ulrich and Huguenard, 1997).

All recordings were conducted in ACSF with the addition of 10 μM DNQX (6,7-dinitroquinoxaline-2,3-dione) and 50 μM DL-APV (DL-2-amino-5-phosphnopentanoic acid; Abcam Biochemicals/Ascent Scientific). Gabazine (50 μM; SR-95531 [6-imino-3-(4-methoxyphenyl)-1(6*H*)-pyridazinebutanoic acid hydrobromide]), a selective $GABA_A$R antagonist, was bath applied (2.5–3 ml/min) to block all $GABA_A$R currents. Gaboxadol, made fresh daily, was applied to slices through the bathing ACSF (2.5–3 ml/min) at a concentration of 1.5 μM or focally at 1 mM to activate high-affinity or synaptic and high-affinity receptors, respectively. Focal delivery of gaboxadol was done through pressure application via a picospritzer pipette (7–9 MΩ) positioned 10–15 μm from the recorded cell (see Fig. 7*F*) with a pressure of 1–3 psi. Mg-ATP, Na-GTP, kynurenic acid, gabazine, and gaboxadol were all purchased from Sigma Aldrich. Neurobiotin was purchased from Vector Laboratories.

Electrophysiology data analysis. Analysis of electrophysiological signals was completed with Clampfit 10.2 (Molecular Devices) and MiniAnalysis (Synaptosoft). Recordings of sIPSCs 180 s long with stable baselines were used to create cumulative distribution histograms of sIPSC amplitude and interevent interval using IGOR Pro 6 (WaveMetrics). Automatic detection of sIPSC events with a threshold of −20 pA and event area threshold of 100 pA · ms was completed using MiniAnalysis 6. For sIPSC kinetic analysis, only events with fast uninterrupted rise times and single exponential decays were aligned on the 50% rise time and averaged for each cell (20–300 events per cell; mean, 59 ± 8). A biexponential function was fitted over the 10–90% decay of the scaled average of all events for each cell. Scaled averaged IPSCs were analyzed for each cell to determine the 10–90% rise time, IPSC half-width, and weighted decay constant value [$\tau_W = (\tau_1 A_1 + \tau_2 A_2)/(A_1 + A_2)$] (Schofield and Huguenard, 2007).

Tonic inhibitory current analysis was performed as described previously (Jia et al., 2005; Glykys and Mody, 2007). Briefly, in Clampfit 10.2, an all-points histogram was created for a 10 s steady-state period in the absence (endogenous) and presence of $GABA_A$R agonists (gaboxadol activated) and/or antagonists (gabazine blockade control). The nonskewed portion of the histogram fitted with a Gaussian function determined the σ value, which was used as the amplitude of the baseline current, obviating the contribution of negative-going sIPSCs. The difference between the mean baseline current amplitude during the control period or during the application of gaboxadol was compared to the baseline current during the application of the antagonist, gabazine. This provided the endogenous and evoked tonic current amplitudes, respectively.

Statistical analyses. Statistical tests used to analyze each data set are noted in the corresponding figure legend and methods section. ANOVAs with a Bonferroni *post hoc* correction were used when multiple comparisons were made. All values are expressed as the mean ± SEM, and statistical comparisons with p values <0.05 are considered significant.

Results

GABA metabolic enzyme, GAD_{67}, is reduced in the cytosolic fraction of MGB

Immunohistochemistry and Western blot analysis of the common marker of GABAergic neurons/terminals and rate-limiting enzyme in GABA production, GAD_{67}, was used to determine the presence of, and age-related changes in, GABA synthesis in young adult and aged MGB, respectively. The presence of dense punctate GAD_{67} labeling supports the presence of putative GABAergic endings in the MGB, presumably from IC and TRN GABAergic neurons (Fig. 1*A*,*B*). Importantly, GAD_{67} labeling appeared reduced in aged tissue (Fig. 1*A*,*B*), which was confirmed using the same GAD_{67} antibody in Western blot assays (Fig. 1*C*,*D*). Quantitative Western blot analysis revealed a significant reduction in the level of GAD_{67} in the cytosolic fraction obtained from the MGB of aged rats relative to the MGB of young adult FBN rats ($n = 9$ young, 9 aged rats; $p = 0.012$; Fig. 1*B*,*C*).

$GABA_A$R density and membrane distribution of $\alpha_4\delta$-subunit-containing $GABA_A$Rs are reduced in aged MGB neurons

A quantitative receptor-binding saturation assay determined the number and affinity of $GABA_A$Rs in young and aged rat MGB neurons. The $GABA_A$R-selective agonist [^{3}H]gaboxadol was used to bind δ-subunit-containing high-affinity $GABA_A$Rs at low concentrations (Friemel et al., 2007; Richardson et al., 2011). Nonlinear regression analysis of [^{3}H]gaboxadol-specific binding indicated that maximal binding density (B_{max}) was significantly reduced (45.5%) in the MGB of aged rats ($n = 5$ young adult, 4 aged rats; $p < 0.0001$; $F_{(2,77)} = 16.35$; Fig. 2*A*). The reduction in [^{3}H]gaboxadol binding density is indicative of a comparable reduction in $GABA_A$R density (Fig. 2). The high affinity of δ-subunit-containing $GABA_A$Rs for gaboxadol indicates that age-related changes in the saturation curve at nanomolar concentrations are likely due to a loss of high-affinity $GABA_A$Rs in aged MGB neurons. Significant age-related changes in mean specific binding density were seen at higher individual concentrations as well (125 nM, $p = 0.033$; 150 nM, $p = 0.016$; 400 nM, $p = 0.0000$; Fig. 2*A*). The affinity of the $GABA_A$R for gaboxadol (dissociation constant, K_d), indicated by the slope of the specific binding-concentration function (Fig. 2*A*, inset), was similar in young adult and aged rats (231.7 and 209.4 in young and aged rats, respectively).

Immunohistochemistry indicates the presence of α_4-subunit-containing $GABA_A$Rs that lack the δ subunit (Fig. 3, merged im-

age, green) and that virtually all δ subunit labeling colocalized with α_4 subunit labeling (Fig. 3, merged image, yellow with little red). The labeling pattern for the α_4 subunit also contrasts that for the δ subunit, in that α_4 subunit labeling is punctate around the soma (near DAPI-labeled nuclei; blue) and also dispersed throughout areas devoid of soma, whereas δ subunit punctate labeling is mostly concentrated near the soma in close proximity to neuronal nuclei (Fig. 3).

Confocal images of MGB neurons from all divisions immunolabeled for α_4 and δ $GABA_AR$ subunits further support the binding results. Aged MGB neurons appear to display decreased punctate surface expression/placement of α_4 and δ $GABA_AR$ subunit protein on aged MGB neurons (Fig. 3). Immunohistochemistry indicates the presence of isolated aggregations of α_4 and δ subunits on aged MGB neurons, which is in contrast to the diffuse punctate somatic labeling for the same subunits in young adult MGB neurons. These observations supported the binding data (Fig. 2) and whole-cell recording data presented below (see Fig. 5), suggesting that α_4δ-subunit-containing $GABA_ARs$ may no longer be distributed on the surface membrane of MGB neurons in aged animals.

Aged MGB neurons are more depolarized and display a reduced $GABA_AR$-mediated tonic Cl^- current

Based on findings reported previously by Richardson et al. (2011), it was postulated that the substantial age-related loss of high-affinity α_4δ-subunit-containing $GABA_ARs$ suggested by [H^3]gaboxadol binding would be reflected by a reduction in tonic $GABA_AR$-mediated Cl^- currents in MGB neurons of aged rats. Whole-cell patch-clamp recordings were obtained from MGB thalamocortical neurons in slices from young adult (3–8 months) and aged (28–32 months) rats. Basic passive and active electrophysiological properties of 10 young adult and nine aged MGB neurons (from two young and two aged FBN rats) from both divisions indicate that they are similar and viable (young, R_{In} = 298 ± 29 MΩ, C = 114.6 ± 12.8 pF, −50.1 ± 0.6 mV AP threshold, 82.5 ± 2.0 mV AP amplitude, 2.3 ± 0.1 ms AP duration; aged, 345 ± 56 MΩ; 88.7 ± 7.5 pF, −49.7 ± 1.4 mV AP threshold, 81.4 ± 2.0 mV AP amplitude, 2.3 ± 0.1 ms AP duration). However, as predicted based on a reduction in [^{3}H]gaboxadol binding and $GABA_AR$ density, aged MGB neurons appeared to be significantly depolarized by an average of 6.3 mV (n = 10 young adult, 9 aged; p = 0.026) (Fig. 4*A*) and demonstrated increased excitability (n = 7 young adult, 7 aged; p = 0.014; Fig. 4*B*) due to

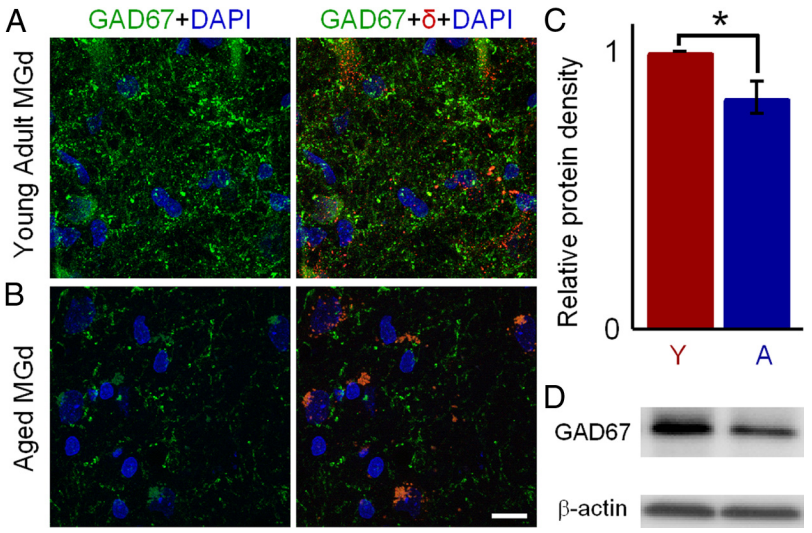

Figure 1. Immunohistochemistry, confocal microscopy, and Western blot indicate cytosolic presynaptic GAD_{67} protein density is reduced with age. ***A***, ***B***, Punctate GAD_{67} immunolabeling (green) in young adult (***A***) and aged (***B***) MGd. Neuronal nuclei were stained with the specific marker, DAPI (blue), and δ-subunit-containing $GABA_ARs$ were labeled with the same antibody used in Figure 3 (red). Results are similar for MGd and MGm. Scale bar, 10 μm. ***C***, Relative protein density from the cytosol fraction obtained from the aged (A) MGB (blue), normalized to levels in the MGB of young FBN (Y, red) rats, matched, and run in parallel, is plotted in the bar graph. Levels of the GABA metabolic enzyme, GAD_{67}, are significantly reduced in the aged MGB. ***D***, Example bands for the GAD_{67} protein/age/fraction combination are at the left with the matched loading control β-actin band below. *$p < 0.01$ (independent-sample t test).

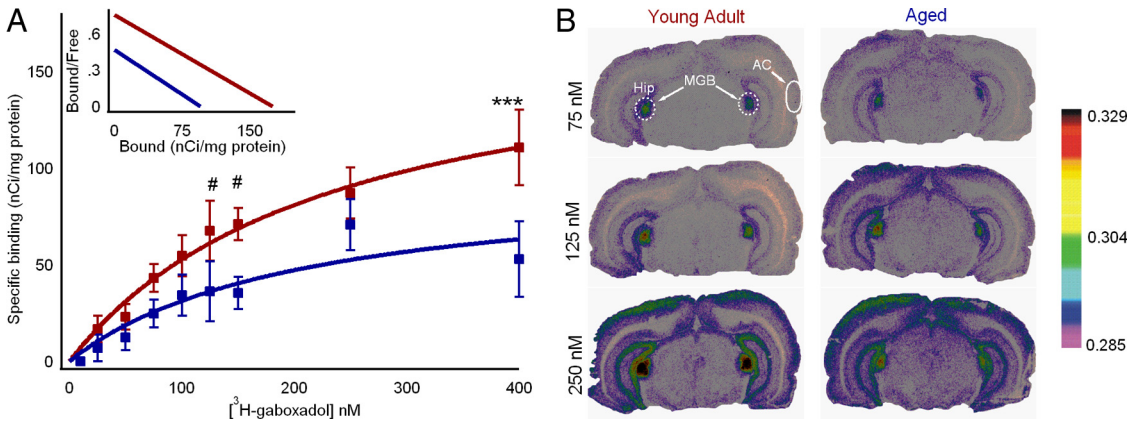

Figure 2. [^{3}H]gaboxadol binding indicates $GABA_AR$ loss with age. ***A***, [^{3}H]gaboxadol (10, 25, 50, 75, 100, 125, 150, 250, and 400 nM) binding isotherm and Scatchard (inset) analyses indicate a 45.5% reduction (174.7 and 96.37 nCi/mg protein in young and aged MGB, respectively) in B_{max} (Scatchard, x-axis) in MGB of coronal sections from young adult (n = 5) and aged (n = 4) FBN rats. Nonlinear regression analysis shows that [^{3}H]gaboxadol binding saturation curves from young adult and aged MGB are significantly different. ***B***, Example autoradiographs of [^{3}H]gaboxadol (75, 125, and 250 nM) binding in young and aged coronal brain sections containing MGB. [^{3}H]gaboxadol binding density differences are most pronounced at 250 nM in this example. On the young 75 nM section, the dotted line outlines the MGB, the solid line outlines auditory cortex (AC), and "Hip" represents hippocampus. Color represents the relative optical density (scale at right). For statistical comparison at each individual concentration, ANOVA with Bonferroni adjustment was used. #$p < 0.05$; ***$p < 0.0001$.

the depolarized resting membrane potential relative to MGB neurons from young rats. When the resting membrane potential of these neurons was adjusted to −65 mV, there was no significant difference in excitability ($p = 0.72$). All neurons were localized to the MGd or MGv as indicated by standard anatomical markers (Fig. 4*F*,G) and displayed putative T-type Ca^{2+}-mediated bursts (arrowheads), indicative of thalamocortical neurons (Fig. 4*D*,*E*). Figure 4, *H* and *I*, gives examples of stellate MGd and tufted MGv neurons recorded from young adult and aged rats, respectively.

To determine age-related changes in high-affinity $GABA_AR$ function, whole-cell recordings were obtained from MGB neurons voltage clamped at −60 mV using a CsCl-based internal solution during the bath application of 1.5 μM gaboxadol, which preferentially activated high-affinity $GABA_ARs$. Subsequent addition of bath applied 50 μM gabazine was used to block all $GABA_ARs$ to reveal/quantify the amplitude of $GABA_AR$-mediated tonic Cl^- current recorded from young adult and aged MGB neurons (Fig. 5*A*). The resulting steady-state gaboxadol-induced inward current and following reduction in steady-state inward current due to gabazine-induced blockade was then used to quantify tonic high-affinity $GABA_AR$ activity (Fig. 5*A*). Gabazine blocked both the gaboxadol-activated tonic current (Fig. 5*A*,*B*) and the endogenously present tonic current (Fig. 5*A*,*C*) as the baseline current became more positive than the baseline current before gaboxadol application (Fig. 5*A*). There were significant 46.2% ($n = 6$ young adult neurons from 4 rats, 8 aged neurons from 5 rats; $p = 0.027$), 53.4% ($n = 8$ young adult neurons from 5 rats, 9 aged neurons from 5 rats; $p = 0.033$), and 50.4% ($n = 16$ young adult neurons from 5 rats, 17 aged neurons from 6 rats; $p = 0.002$) reductions in high-affinity $GABA_AR$-mediated inhibitory current in nonlemniscal MGd, lemniscal MGv, and all MGB neurons, respectively (Fig. 5*B*). This reduction in $GABA_AR$-mediated tonic Cl^- current amplitude was in direct agreement with the 45.5% decrease in [^{3}H]gaboxadol binding (B_{max}). Similarly, the endogenous tonic current present in MGB neurons due to the ambient concentration of GABA (difference between baseline current before gaboxadol application and after gabazine application) was significantly reduced in MGB neurons from aged rats by 75.6% ($n = 8$ young adult, 9 aged; $p =$

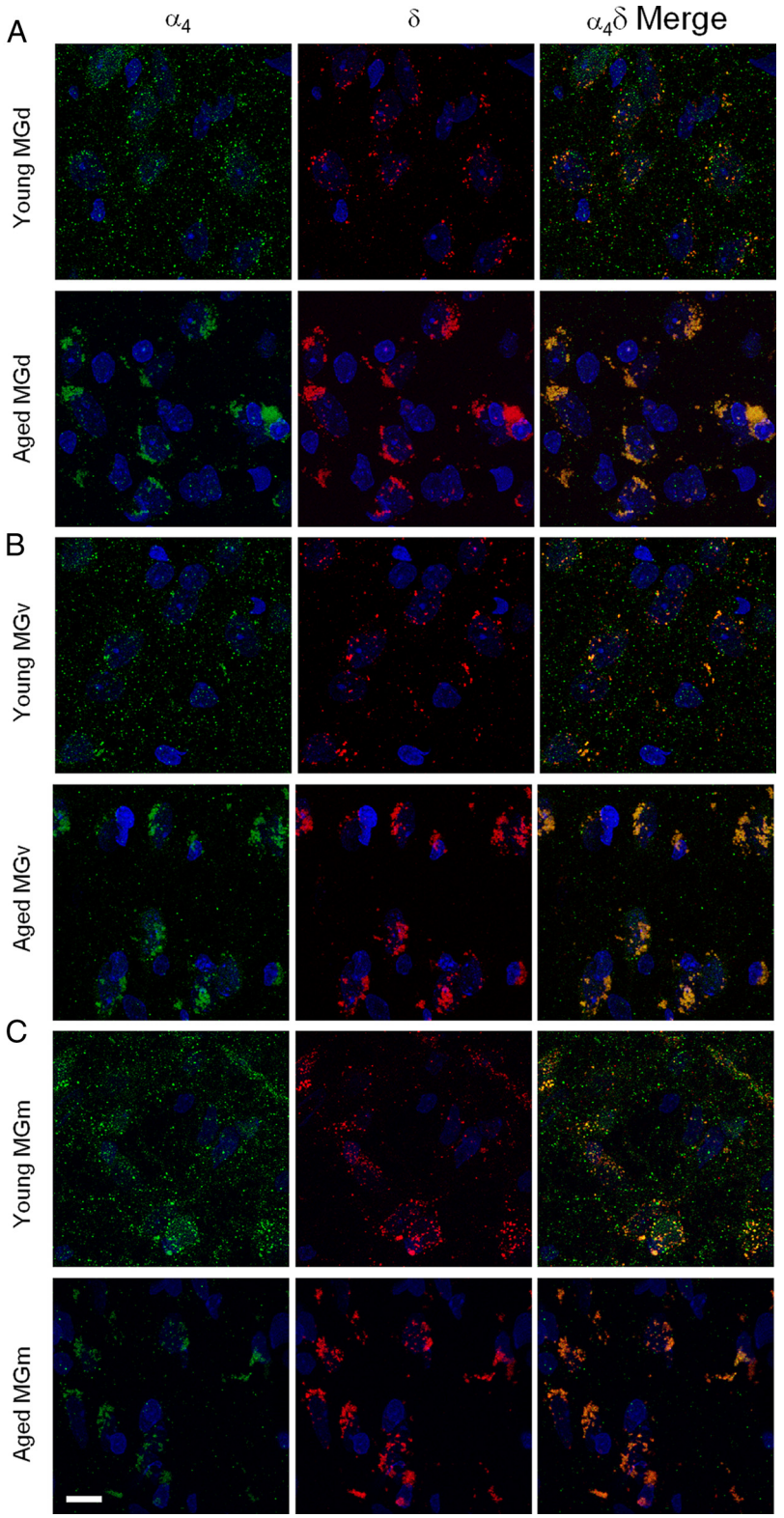

Figure 3. $GABA_AR$ α_4 and δ subunit distribution in MGB neurons is disrupted with age. ***A–C***, Fluorescent immunolabeling of high-affinity $GABA_AR$ constructs, the α_4 (left, green) and δ (middle, red; right, yellow) subunits in young adult dorsal (***A***), ventral (***B***), and medial (***C***) divisions of MGB neurons (top rows), indicates a punctate, diffuse, evenly distributed and mostly somatic localization on MGB neurons. The distribution of α_4 and δ subunit labeling in aged dorsal (***A***), ventral (***B***), and medial (***C***) divisions of MGB neurons (bottom rows) appears less punctate and evenly distributed and more confined to aggregations near/within the soma. In images from young adult MGB divisions, labeling of α_4 subunits (left, green) is evenly distributed throughout each region, regardless of the location of soma, as identified by DAPI (blue) labeling of neuronal nuclei, and is not always colocalized with the δ (middle, red; right, yellow). In contrast, δ subunit labeling (middle, red) always colocalizes with α_4 (left, green; right, yellow) and is most commonly concentrated on the soma, with little labeling away from DAPI-labeled nuclei (blue) compared to α_4 subunit labeling. Scale bar, 10 μm.

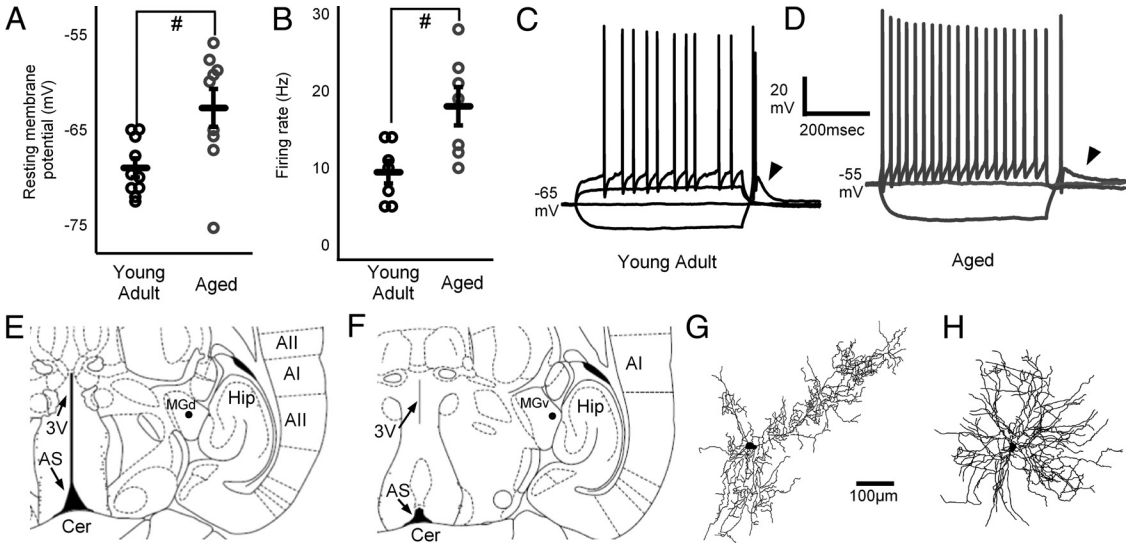

Figure 4. Depolarization and enhanced excitability of aged MGB neurons and anatomical localization. ***A***, ***B***, Only resting membrane potential and AP frequency (indicated by firing rate in response to the first 50 pA step that initiated action potentials in cells with a sustained firing pattern) were significantly elevated with age. $^{\#}p < 0.05$ (independent-sample *t* test). ***C***, ***D***, Representative examples of recordings from young adult (***C***, black) and aged (***D***, gray) MGB. ***E***, Drawing of a horizontal rat brain slice containing MGd (Paxinos and Watson, 1998), where the midbrain has not yet fused with the Aqueduct of Sylvius (AS) and the third ventricle (3V) remains continuous. The black dot represents the location of the young adult neurobiotin-filled stellate neuron drawn in ***G***. ***F***, Drawing of a horizontal rat brain slice ventral to ***E*** where left and right hemispheres have fused, separating the AS and 3V. The black dot represents the location of the aged tufted neuron drawn in ***H***. Both neurons are oriented as they would appear in the corresponding anatomical drawings with the rostral end up. The scale bar applies to both neurons. Cer, Cerebellum; Hip, hippocampus; AI, primary auditory cortex; AII, secondary auditory cortex.

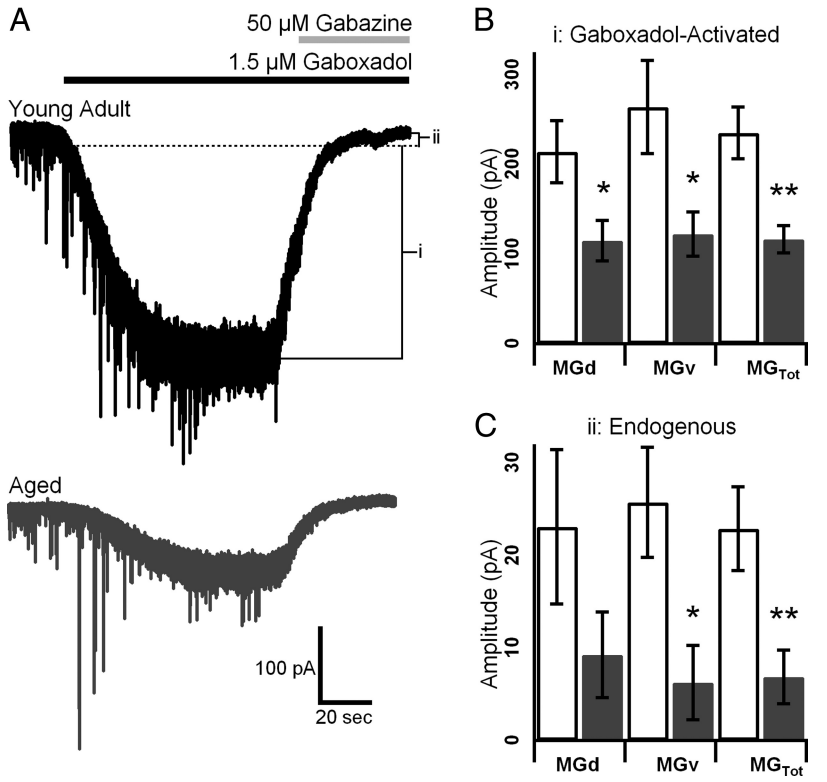

Figure 5. $GABA_AR$-mediated tonic inhibitory currents are reduced with age. ***A***, Raw sample trace recorded from a young adult (top, black) and an aged (bottom, gray) MGB neuron during the application of 1.5 μM gaboxadol and subsequent blockade of synaptic and high-affinity $GABA_ARs$ with 50 μM gabazine. Calibration applies to both traces. ***B***, ***C***, Gaboxadol-activated (***B***) and endogenous (***C***) high-affinity $GABA_AR$-mediated tonic current amplitudes from MGd, MGv, and all MGB (MG_{Tot}) neurons. ***B*** shows the tonic current amplitude difference between baseline current activated by the application of 1.5 μM gaboxadol and the baseline current in the presence of 50 μM gabazine, which blocks all $GABA_ARs$ (the gaboxadol-activated current), whereas ***C*** shows the tonic current amplitude difference between the baseline current before the addition of gaboxadol and after the application of gabazine (the endogenous tonic current). Open bars, Young adult; gray bars, aged rats. $^{*}p < 0.05$; $^{**}p < 0.01$ (independent-sample *t* tests).

0.015) in MGv neurons and 69.9% (n = 16 young adult, 17 aged; $p = 0.009$) for all MGB neurons, with a similar but nonsignificant trend in MGd neurons (59.9%; $n = 6$ young adult, 8 aged; $p = 0.186$; Fig. 5*C*). This age-related decrease in endogenous inhibitory tone supports the observed depolarized resting membrane potential and increased excitability of aged MGB neurons (Fig. 4*A–D*).

Synaptic inhibitory neurotransmission is differentially altered in lemniscal and nonlemniscal MGB neurons with age

Whole-cell recordings of sIPSC in MGB neurons held at −60 mV using a CsCl-based internal solution were analyzed to determine age-related changes in inhibitory synaptic transmission (Fig. 6*A*). Cumulative amplitude and interevent interval distributions of sIPSCs demonstrate an age-related decrease in sIPSC amplitude [$p < 0.00001$; critical value (CV), 0.12; $D = 0.42$] and frequency ($p < 0.00001$; CV, 0.07; $D = 0.28$) in the nonlemniscal MGd ($n = 10$ young adult neurons from 7 rats, 13 aged neurons from 6 rats) and an opposing increase in sIPSC amplitude ($p < 0.00001$; CV, 0.12; $D = 0.56$) and frequency ($p < 0.00001$; CV, 0.073; $D = 0.28$) in the lemniscal MGv ($n = 10$ young adult neurons from 6 rats, 11 aged neurons from 5 rats; Fig. 6*B*). This discrepancy between MGv and MGd neurons may underlie a difference in the primary sources of synaptic inhi-

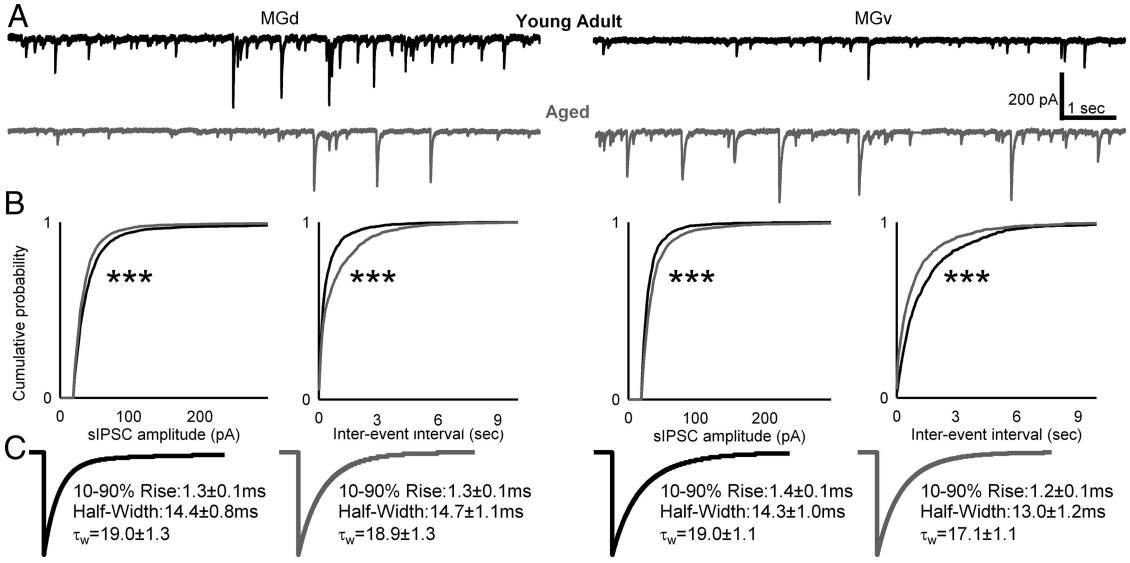

Figure 6. Synaptic $GABA_AR$ inhibition changes differentially in nonlemniscal and lemniscal MGB neurons with age. ***A***, Top traces are representative examples of spontaneous IPSCs recorded from nonlemniscal MGd (left) and lemniscal MGv (right) neurons of a young adult (black, top) and an aged (gray, bottom) FBN rat. ***B***, Corresponding cumulative probability histograms of IPSC amplitudes and interevent intervals (black, young adult; gray, aged) represent an age-related decrease in amplitude (left) and frequency (right) in MGd neurons (***A***, left) and opposing increase in amplitude (left) and frequency (right) in MGv neurons (***A***, right). All functions are the average function of single functions constructed for each individual neuron. ***C***, sIPSC kinetics do not change with age. Average normalized IPSC trace corresponding to the representative trace in ***A***. Values for 10–90% rise time, half-width, and weighted decay constant (τ_W) under each averaged IPSC are the average ± SEM values from the average normalized IPSC from each neuron within that group. There was no significant difference between these measures of ISPC kinetic properties for young adult and aged MGd or MGv neurons. Independent-sample *t* tests and Kolmogorov–Smirnov tests were used to test for significant age-related differences between the measures of IPSC kinetics and amplitude and interevent interval distributions. $^{***}p < 0.0001$.

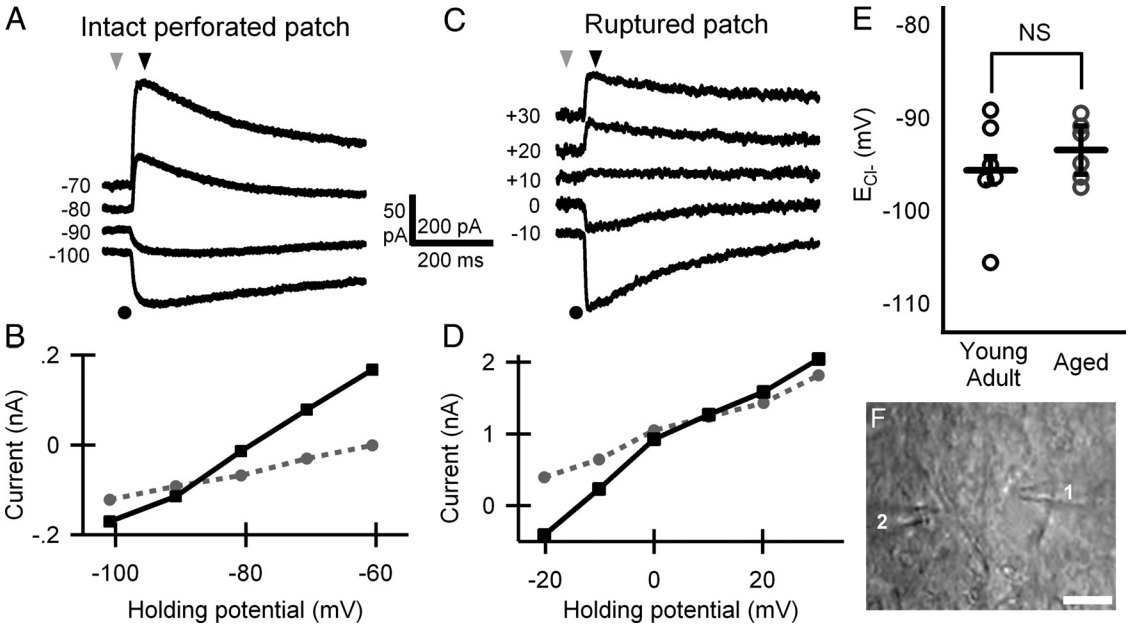

Figure 7. MGB neuron $[Cl^-]_i$ remains constant with age. ***A***, ***C***, Typical examples of current traces recorded from an aged MGB neuron during perforated patch recording (***A***) and after rupturing the patch to gain whole-cell access (***C***). The holding potential for each trace is indicated to the left. The dot (bottom left) represents the focal application of 1 mM gaboxadol. Calibration: ***A***, 250 ms, 50 pA; ***C***, 250 ms, 200 pA. ***B***, ***D***, *I–V* plots before and after the application of gaboxadol during perforated patch (***B***) and whole-cell (***D***) configurations corresponding to ***A*** and ***C***, respectively. The black lines represent values at black arrows, and gray dotted lines represent values at gray arrows in ***A*** and ***C***, respectively. The intersection of solid and dotted lines represents the theoretical GABA/Cl^- reversal potential. ***E***, GABA/Cl^- equilibrium potentials for young adult ($n = 6$; black open circles) and aged ($n = 6$; gray open circles) MGB neurons. Black lines with bars are the mean ± SEM. NS, Not significant (independent-sample *t* test was used). ***F***, Image of aged MGB neuron with recording (1) and application (2) pipettes placed ~15 μm from the soma. Scale bar, 10 μm.

bition, which are yet to be described. While sIPSC amplitude and frequency were altered in aged MGB neurons, the magnitude of this change was small relative to the change in high-affinity $GABA_AR$-mediated tonic currents, but may still have negative consequences in stimulus coding by MGB neurons.

No significant changes were detected in sIPSC kinetics (Fig. 6*C*) of aged MGB neurons [$n = 11$ young adult, 12 aged MGd neurons; $n = 11$ young adult, 10 aged MGv neurons; 10–90% rise time, $p = 0.679$ for MGd, $p = 0.497$ for MGv; half-width, $p = 0.887$ for MGd, $p = 0.427$ for MGv; τ_W (weighted decay

constant), $p = 0.937$ for MGd, $p = 0.235$ for MGv; independent-sample t test].

The Cl^- equilibrium potentials of young adult and aged MGB neurons are similar

The gramicidin-perforated patch-clamp method was used to obtain access to neuronal cytosol and control the membrane potential without altering the $[Cl^-]_i$ (Fig. 7). Focal gaboxadol (1 mM) application evoked $GABA_A$R-mediated currents at a range of holding potentials to estimate the reversal potential for $GABA_A$R-mediated Cl^- currents (Fig. 7*A*,*C*,*F*). The intersection of the *I–V* curves obtained before and immediately after gaboxadol application gave an estimation of the Cl^- equilibrium potential (Fig. 7*B*,*D*), which was not significantly different ($n = 6$ young adult neurons from 4 rats, 6 aged neurons from 3 rats; $p = 0.436$) between MGB neurons of young adult (-95.7 ± 2.3 mV) and aged rats (-93.5 ± 1.3 mV; corrected for the electrode/bath 3.5 mV LJP, but not the perforated patch potential; Fig. 7*E*). Rupture of the perforated patch with negative pressure resulted in a change of E_{Cl^-} (-3.9 ± 2.8 mV), which was near the theoretical value calculated using the Nernst equation (-2.4 mV) in 100% of cells tested (eight of eight).

Discussion

These data demonstrate a significant age-dependent deficit in the GABAergic inhibitory tone within MGB neurons, caused by reduced/altered expression and/or activation of $GABA_A$ receptors, particularly those that mediate tonic inhibition in the FBN rat. Demonstration of an age-related loss of high affinity (often referred to as extrasynaptic) $GABA_A$Rs mediating tonic inhibition was supported by altered neurochemical markers, which may partially explain auditory coding and/or gating deficits in the elderly. Importantly, if similar maladaptive age-related $GABA_A$R changes are found in other sensory thalamic nuclei, this could explain age-related deficiencies in sensory gating, attention, and slow-wave sleep (Steriade et al., 1993; Guillery et al., 1998; Belelli et al., 2009; Herd et al., 2009; Crowley, 2011).

The present study quantitatively addressed the functional correlates of the age-related changes in receptor binding and immunohistochemistry in the MGB using whole-cell recordings obtained from MGB neurons in young adult and aged brain slices. [^{3}H]gaboxadol binding data (Fig. 2) suggested an age-related plasticity of $GABA_A$Rs. The binding studies were further supported by the confocal images, which suggested age-related changes in $\alpha_4\delta$-subunit-containing $GABA_A$Rs expressed on the surface membrane of young adult MGB neurons, in contrast with isolated aggregations of these subunits in aged MGB neurons (Fig. 3). Similarly, altered inhibitory synaptic function and changes in inhibitory receptor cytosol/membrane location have been demonstrated in auditory cortical pyramidal neurons in developmentally hearing-impaired gerbils (Sanes and Kotak, 2011). Together, these results suggest that certain $GABA_A$R constructs found in adult MGB, may not be normally trafficked, anchored, and present in the cell membrane of MGB thalamocortical neurons of aged animals (for review, see Wang et al., 2009; Tyagarajan and Fritschy, 2010). The age-related reduction in GAD_{67} expression, likely representing presynaptic terminals as described previously (Winer and Larue, 1988; Bartlett et al., 2000; Smith et al., 2012), is similar to what has been observed in other central auditory structures and suggests a decrease in GABA production and, thus, release (Caspary et al., 2008). This would likely alter ambient GABA levels activating high-affinity δ-subunit-containing $GABA_A$Rs. These changes in neurochemical markers of inhibitory neurotransmission in MGB are in agreement with age-related changes in presynaptic and postsynaptic glycinergic and GABAergic markers identified in central auditory structures and nonauditory cortex, cerebellum, and hippocampus (Rissman et al., 2007; Caspary et al., 2008). Determination of the membrane surface synaptic/extrasynaptic localization of δ-subunit-containing $GABA_A$Rs on MGB neurons will require further study (e.g., immunogold electron microscopy).

Results from whole-cell recordings show that both slow/tonic and fast/phasic GABAergic inhibitions are negatively impacted in the aged auditory thalamus (Figs. 5, 6). The dramatic age-related decrease in high-affinity $GABA_A$R-mediated tonic inhibition reflects a maladaptive age-related homeostatic plasticity in the sensory thalamus. Similar changes, suggestive of high-affinity $GABA_A$R pathology, have been documented in epilepsy, tinnitus, and traumatic brain injury (Cope et al., 2009; Yang et al., 2011; Gupta et al., 2012). Loss of high-affinity $GABA_A$Rs may be significant, as Cope et al. (2005) indicated that up to 90% of thalamocortical cells' inhibitory tones may be mediated by high-affinity $GABA_A$Rs, which regulate the tonic to burst mode transition in the thalamus and set the resting membrane potential and input resistance, collectively shaping the output of the thalamus (Cope et al., 2005; Jia et al., 2008).

The age-related decrease in sIPSC amplitude and frequency observed in the nonlemniscal MGd with an opposing shift in the distributions for lemniscal MGv neurons could have two possible explanations: (1) the horizontal cutting angle may have severed some inhibitory fibers from the IC or TRN, which may bias the results in one direction, and/or (2) the dominant sources of synaptic inhibition to the MGd and MGv may be different and are differentially impacted by aging. One possibility may be that the documented age-related increases in the activity of the IC could have a greater impact on the MGv than MGd (Caspary et al., 2008).

Evaluation of other passive (input resistance, capacitance) and active (AP amplitude, duration, threshold, E_{Cl^-}) membrane properties revealed that while inhibition seems to be altered in the aged MGB, many of these other properties remain conserved regardless of age. In addition to whole-cell recordings of basic membrane properties, gramicidin-perforated patch-clamp recordings were used to approximate the Cl^- equilibrium potential (E_{Cl^-}) of young and aged MGB neurons, providing an original estimation of the E_{Cl^-} in adult sensory thalamic neurons. More importantly, age-related changes in Cl^- homeostasis due to fluctuations in the KCC_2 transporter, which maintains $[Cl^-]_i$, could counter age-related reductions in membrane bound $GABA_A$R function identified in experiments described above. However, E_{Cl^-} was similar in MGB neurons of young adult and aged rats, suggesting that the decrease/change in GABAergic inhibitory function or inhibitory tone was not compensated for by a change in the $[Cl^-]_i$ (Fig. 7). These data suggest that aging, *de novo* or as a result of deafferentation, may not simply alter neural function on a global scale, but rather results in subtle changes in specific neuronal and network properties that may have noticeable correlates at the level of the whole organism. Notably, the E_{Cl^-} values for MGB neurons are more negative than would be expected, but were not corrected for the unknown perforated patch potential. Regardless, the E_{Cl^-} values follow the trend of hyperpolarized E_{Cl^-} values of somatosensory thalamic neurons (-81 mV) of 9- to 12-d-old rats reported previously (Ulrich and Huguenard, 1997).

Tonic $GABA_A$R-mediated inhibition of thalamic neurons results in hyperpolarization of the resting membrane potential,

thus reducing neuronal excitability. This property of tonic $GABA_A$R-mediated inhibition improves coding fidelity in the cerebellum by enhancing the signal-to-noise ratio and would presumably have a similar effect, reducing jitter in the auditory thalamus (Richardson et al., 2011; Duguid et al., 2012). $GABA_A$R-mediated tonic inhibition also influences thalamocortical transmission by switching thalamic neuron firing modes from tonic to burst (Cope et al., 2005). High-affinity δ-subunit-containing $GABA_A$Rs mediating a persistent hyperpolarization of thalamocortical neuronal membrane potential results in the deinactivation of low-threshold Ca^{2+} ion channels, necessary for thalamic bursting/oscillations involved in slow-wave sleep, arousal, and attention (Steriade et al., 1993; Guillery et al., 1998; Cope et al., 2005; Bright et al., 2007; Richardson et al., 2011). Moreover, bursting of sensory thalamic neurons and corticothalamic oscillations are associated with increased GABAergic input from the TRN, which is involved in sensory gating and attention and sleep states (Crick, 1984; Steriade et al., 1993; Guillery et al., 1998; Pinault, 2004).

However, this interaction may be unique to the MGB due to the increased incidence of the depolarizing I_h current in MGv neurons, which may counter moderate increases in tonic inhibition in the lemniscal MGv, but not the MGd (Bartlett and Smith, 1999). As a result, MGd neurons may be more hyperpolarized when ambient GABA concentrations increase. In fact, MGd neurons preferentially participate in thalamocortical oscillations and respond with bursts more readily *in vivo* than MGv neurons (Steriade et al., 1993; Bartlett and Smith, 1999; He and Hu, 2002; He, 2003). Therefore, the nonlemniscal MGd, which selectively receives input from giant GABAergic terminals, may play an important role in auditory gating and attention, while the lemniscal ventral division serves in a more direct relay capacity (Winer et al., 1999; Richardson et al., 2011). In fact, compared to single-spike responses, burst responses of thalamocortical relay cells double the probability of eliciting a response in cortical neurons (Swadlow and Gusev, 2001), further indicating the importance of hyperpolarization-induced burst in the MGB in sensory gating/filtering (Cope et al., 2005; Richardson et al., 2012).

The essential role of inhibition in auditory scene coding, which is deficient in the elderly, has been characterized previously and is described above. The loss of tonic inhibition would depolarize the resting potential of MGB neurons closer to action potential threshold, increasing excitability and temporal uncertainty, and decreasing coding fidelity with age (Duguid et al., 2012). This effect may contribute to the depolarized state and increased excitability in the subset of MGB neurons recorded from aged rats in current-clamp recordings (Fig. 4). Previously, a link between the loss of inhibition and auditory coding was demonstrated using acoustic behavioral training, which improved novelty detection and temporal coding and was directly correlated with enhanced GABAergic markers in auditory cortical neurons of aged rats (de Villers-Sidani et al., 2010). Similarly, improved temporal coding (gap detection behavioral task) in aged gerbils was seen following enhancement of ambient GABA levels by systemic administration of vigabatrin, a GABA-transaminase inhibitor (Gleich et al., 2003). This effect was likely due, in part, to the enhancement of tonic inhibition via high-affinity $GABA_A$Rs.

In a broader scope, if the age-related loss of high-affinity $GABA_A$R-mediated tonic inhibition generalizes to all sensory thalamus, which is essential for the maintenance of thalamic oscillations underlying slow-wave sleep, this may not only explain the deficiencies the elderly experience in sensory processing during attention-demanding tasks, but also slow-wave sleep (Alain and Woods, 1999; Crowley, 2011). In fact, 30 d treatment with gaboxadol improves the duration of slow-wave sleep in the elderly suffering from insomnia probably through a mechanism involving thalamic high-affinity $GABA_A$Rs (Lankford et al., 2008). These types of pharmacotherapy target high-affinity $GABA_A$Rs and ambient GABA levels, restoring levels of thalamic tonic inhibition following the age-related loss of high-affinity $GABA_A$Rs in the thalamus documented here. Similar treatments may be the beginning of a therapeutic strategy to improve attention, quality of sleep and result in improved overall mental health in the elderly.

References

Alain C, Woods DL (1999) Age-related changes in processing auditory stimuli during visual attention: evidence for deficits in inhibitory control and sensory memory. Psychol Aging 14:507–519. CrossRef Medline

Anderson S, Parbery-Clark A, White-Schwoch T, Kraus N (2012) Aging affects neural precision of speech encoding. J Neurosci 32:14156–14164. CrossRef Medline

Bartlett EL, Smith PH (1999) Anatomic, intrinsic, and synaptic properties of dorsal and ventral division neurons in rat medial geniculate body. J Neurophysiol 81:1999–2016. Medline

Bartlett EL, Stark JM, Guillery RW, Smith PH (2000) Comparison of the fine structure of cortical and collicular terminals in the rat medial geniculate body. Neuroscience 100:811–828. CrossRef Medline

Belelli D, Peden DR, Rosahl TW, Wafford KA, Lambert JJ (2005) Extrasynaptic GABAA receptors of thalamocortical neurons: a molecular target for hypnotics. J Neurosci 25:11513–11520. CrossRef Medline

Belelli D, Harrison NL, Maguire J, Macdonald RL, Walker MC, Cope DW (2009) Extrasynaptic GABAA receptors: form, pharmacology, and function. J Neurosci 29:12757–12763. CrossRef Medline

Bright DP, Aller MI, Brickley SG (2007) Synaptic release generates a tonic GABA(A) receptor-mediated conductance that modulates burst precision in thalamic relay neurons. J Neurosci 27:2560–2569. CrossRef Medline

Caspary DM, Palombi PS, Hughes LF (2002) GABAergic inputs shape responses to amplitude modulated stimuli in the inferior colliculus. Hear Res 168:163–173. CrossRef Medline

Caspary DM, Schatteman TA, Hughes LF (2005) Age-related changes in the inhibitory response properties of dorsal cochlear nucleus output neurons: role of inhibitory inputs. J Neurosci 25:10952–10959. CrossRef Medline

Caspary DM, Ling L, Turner JG, Hughes LF (2008) Inhibitory neurotransmission, plasticity and aging in the mammalian central auditory system. J Exp Biol 211:1781–1791. CrossRef Medline

Chandra D, Jia F, Liang J, Peng Z, Suryanarayanan A, Werner DF, Spigelman I, Houser CR, Olsen RW, Harrison NL, Homanics GE (2006) GABAA receptor alpha 4 subunits mediate extrasynaptic inhibition in thalamus and dentate gyrus and the action of gaboxadol. Proc Natl Acad Sci U S A 103:15230–15235. CrossRef Medline

Chen QC, Jen PH (2000) Bicuculline application affects discharge patterns, rate-intensity functions, and frequency tuning characteristics of bat auditory cortical neurons. Hear Res 150:161–174. CrossRef Medline

Cope DW, Hughes SW, Crunelli V (2005) GABAA receptor-mediated tonic inhibition in thalamic neurons. J Neurosci 25:11553–11563. CrossRef Medline

Cope DW, Di Giovanni G, Fyson SJ, Orbán G, Errington AC, Lorincz ML, Gould TM, Carter DA, Crunelli V (2009) Enhanced tonic GABAA inhibition in typical absence epilepsy. Nat Med 15:1392–1398. CrossRef Medline

Cotillon-Williams N, Huetz C, Hennevin E, Edeline JM (2008) Tonotopic control of auditory thalamus frequency tuning by reticular thalamic neurons. J Neurophysiol 99:1137–1151. CrossRef Medline

Crick F (1984) Function of the thalamic reticular complex: the searchlight hypothesis. Proc Natl Acad Sci U S A 81:4586–4590. CrossRef Medline

Crowley K (2011) Sleep and sleep disorders in older adults. Neuropsychol Rev 21:41–53. CrossRef Medline

Cruickshanks KJ, Wiley TL, Tweed TS, Klein BE, Klein R, Mares-Perlman JA, Nondahl DM (1998) Prevalence of hearing loss in older adults in Beaver Dam, Wisconsin. The epidemiology of hearing loss study. Am J Epidemiol 148:879–886. CrossRef Medline

de Villers-Sidani E, Alzghoul L, Zhou X, Simpson KL, Lin RC, Merzenich MM

(2010) Recovery of functional and structural age-related changes in the rat primary auditory cortex with operant training. Proc Natl Acad Sci U S A 107:13900–13905. CrossRef Medline

Duguid I, Branco T, London M, Chadderton P, Häusser M (2012) Tonic inhibition enhances fidelity of sensory information transmission in the cerebellar cortex. J Neurosci 32:11132–11143. CrossRef Medline

Edeline JM (2011) Physiological properties of neurons in the medial geniculate body. In: The auditory cortex (Winer JA, Schreiner CE, eds), pp 251–274. New York: Springer.

Friemel A, Ebert B, Hutson PH, Brust P, Nieber K, Deuther-Conrad W (2007) Postnatal development and kinetics of [3H]gaboxadol binding in rat brain: in vitro homogenate binding and quantitative autoradiography. Brain Res 1170:39–47. CrossRef Medline

Gleich O, Hamann I, Klump GM, Kittel M, Strutz J (2003) Boosting GABA improves impaired auditory temporal resolution in the gerbil. Neuroreport 14:1877–1880. CrossRef Medline

Glykys J, Mody I (2007) The main source of ambient GABA responsible for tonic inhibition in the mouse hippocampus. J Physiol 582:1163–1178. CrossRef Medline

Gońdon-Salant S, Fitzgibbons PJ (1993) Temporal factors and speech recognition performance in young and elderly listeners. J Speech Hear Res 36:1276–1285. Medline

Gońdon-Salant S, Frisina RD, Fay RR, Popper AN, eds (2010) The aging auditory system. New York: Springer.

Guillery RW, Feig SL, Lozsádi DA (1998) Paying attention to the thalamic reticular nucleus. Trends Neurosci 21:28–32. CrossRef Medline

Gupta A, Elgammal FS, Proddutur A, Shah S, Santhakumar V (2012) Decrease in tonic inhibition contributes to increase in dentate semilunar granule cell excitability after brain injury. J Neurosci 32:2523–2537. CrossRef Medline

He J (2003) Slow oscillation in non-lemniscal auditory thalamus. J Neurosci 23:8281–8290. Medline

He J, Hu B (2002) Differential distribution of burst and single-spike responses in auditory thalamus. J Neurophysiol 88:2152–2156. Medline

Herd MB, Foister N, Chandra D, Peden DR, Homanics GE, Brown VJ, Balfour DJ, Lambert JJ, Belelli D (2009) Inhibition of thalamic excitability by 4,5,6,7-tetrahydroisoxazolo[4,5-c]pyridine-3-ol: a selective role for delta-GABA(A) receptors. Eur J Neurosci 29:1177–1187. CrossRef Medline

Humes LE, Kewley-Port D, Fogerty D, Kinney D (2010) Measures of hearing threshold and temporal processing across the adult lifespan. Hear Res 264:30–40. CrossRef Medline

Jia F, Pignataro L, Schofield CM, Yue M, Harrison NL, Goldstein PA (2005) An extrasynaptic GABAA receptor mediates tonic inhibition in thalamic VB neurons. J Neurophysiol 94:4491–4501. CrossRef Medline

Jia F, Yue M, Chandra D, Keramidas A, Goldstein PA, Homanics GE, Harrison NL (2008) Taurine is a potent activator of extrasynaptic GABAA receptors in the thalamus. J Neurosci 28:106–115. CrossRef Medline

Juarez-Salinas DL, Engle JR, Navarro XO, Recanzone GH (2010) Hierarchical and serial processing in the spatial auditory cortical pathway is degraded by natural aging. J Neurosci 30:14795–14804. CrossRef Medline

Kimura A, Imbe H, Donishi T, Tamai Y (2007) Axonal projections of single auditory neurons in the thalamic reticular nucleus: implications for tonotopy-related gating function and cross-modal modulation. Eur J Neurosci 26:3524–3535. CrossRef Medline

Lankford DA, Corser BC, Zheng YP, Li Z, Snavely DB, Lines CR, Deacon S (2008) Effect of gaboxadol on sleep in adult and elderly patients with primary insomnia: results from two randomized, placebo-controlled, 30-night polysomnography studies. Sleep 31:1359–1370. Medline

Lipman RD, Chrisp CE, Hazzard DG, Bronson RT (1996) Pathologic characterization of brown Norway, brown Norway x Fischer 344, and Fischer 344 x brown Norway rats with relation to age. J Gerontol A Biol Sci Med Sci 51:B54–B59. Medline

Lister J, Besing J, Koehnke J (2002) Effects of age and frequency disparity on gap discrimination. J Acoust Soc Am 111:2793–2800. CrossRef Medline

Milbrandt JC, Caspary DM (1995) Age-related reduction of [3H]strychnine binding sites in the cochlear nucleus of the Fischer 344 rat. Neuroscience 67:713–719. CrossRef Medline

Mortensen M, Ebert B, Wafford K, Smart TG (2010) Distinct activities of GABA agonists at synaptic- and extrasynaptic-type GABAA receptors. J Physiol 588:1251–1268. CrossRef Medline

Palombi PS, Caspary DM (1992) GABAA receptor antagonist bicuculline alters response properties of posteroventral cochlear nucleus neurons. J Neurophysiol 67:738–746. Medline

Paxinos W, Watson C (1998) The rat brain in stereotaxic coordinates. San Diego: Academic.

Peruzzi D, Bartlett E, Smith PH, Oliver DL (1997) A monosynaptic GABAergic input from the inferior colliculus to the medial geniculate body in rat. J Neurosci 17:3766–3777. Medline

Pinault D (2004) The thalamic reticular nucleus: structure, function and concept. Brain Res Brain Res Rev 46:1–31. Medline

Pirker S, Schwarzer C, Wieselthaler A, Sieghart W, Sperk G (2000) GABA(A) receptors: immunocytochemical distribution of 13 subunits in the adult rat brain. Neuroscience 101:815–850. CrossRef Medline

Richardson BD, Ling LL, Uteshev VV, Caspary DM (2011) Extrasynaptic GABA(A) receptors and tonic inhibition in rat auditory thalamus. PLoS ONE 6:e16508. CrossRef Medline

Richardson BD, Brozoski TJ, Ling LL, Caspary DM (2012) Targeting inhibitory neurotransmission in tinnitus. Brain Res 1485:77–87. CrossRef Medline

Rissman RA, De Blas AL, Armstrong DM (2007) GABA(A) receptors in aging and Alzheimer's disease. J Neurochem 103:1285–1292. CrossRef Medline

Sanes DH, Kotak VC (2011) Developmental plasticity of auditory cortical inhibitory synapses. Hear Res 279:140–148. CrossRef Medline

Schofield CM, Huguenard JR (2007) GABA affinity shapes IPSCs in thalamic nuclei. J Neurosci 27:7954–7962. CrossRef Medline

Sieghart W, Sperk G (2002) Subunit composition, distribution and function of GABA(A) receptor subtypes. Curr Top Med Chem 2:795–816. CrossRef Medline

Smith PH, Uhlrich DJ, Manning KA, Banks MI (2012) Thalamocortical projections to rat auditory cortex from the ventral and dorsal divisions of the medial geniculate nucleus. J Comp Neurol 520:34–51. CrossRef Medline

Snell KB (1997) Age-related changes in temporal gap detection. J Acoust Soc Am 101:2214–2220. CrossRef Medline

Steriade M, McCormick DA, Sejnowski TJ (1993) Thalamocortical oscillations in the sleeping and aroused brain. Science 262:679–685. CrossRef Medline

Suga N, Zhang Y, Yan J (1997) Sharpening of frequency tuning by inhibition in the thalamic auditory nucleus of the mustached bat. J Neurophysiol 77:2098–2114. Medline

Sur C, Farrar SJ, Kerby J, Whiting PJ, Atack JR, McKernan RM (1999) Preferential coassembly of alpha4 and delta subunits of the gamma-aminobutyric acidA receptor in rat thalamus. Mol Pharmacol 56:110–115. Medline

Suta D, Rybalko N, Pelánová J, Popelář J, Syka J (2011) Age-related changes in auditory temporal processing in the rat. Exp Gerontol 46:739–746. CrossRef Medline

Swadlow HA, Gusev AG (2001) The impact of 'bursting' thalamic impulses at a neocortical synapse. Nat Neurosci 4:402–408. CrossRef Medline

Takahashi GA, Bacon SP (1992) Modulation detection, modulation masking, and speech understanding in noise in the elderly. J Speech Hear Res 35:1410–1421. Medline

Tremblay KL, Piskosz M, Souza P (2003) Effects of age and age-related hearing loss on the neural representation of speech cues. Clin Neurophysiol 114:1332–1343. CrossRef Medline

Tyagarajan SK, Fritschy JM (2010) GABA(A) receptors, gephyrin and homeostatic synaptic plasticity. J Physiol 588:101–106. CrossRef Medline

Ulrich D, Huguenard JR (1997) Nucleus-specific chloride homeostasis in rat thalamus. J Neurosci 17:2348–2354. Medline

Walker MC, Semyanov A (2008) Regulation of excitability by extrasynaptic GABA(A) receptors. Results Probl Cell Differ 44:29–48. CrossRef Medline

Walton JP (2010) Timing is everything: temporal processing deficits in the aged auditory brainstem. Hear Res 264:63–69. CrossRef Medline

Wang H, Turner JG, Ling L, Parrish JL, Hughes LF, Caspary DM (2009) Age-related changes in glycine receptor subunit composition and binding in dorsal cochlear nucleus. Neuroscience 160:227–239. CrossRef Medline

Winer JA, Larue DT (1988) Anatomy of glutamic acid decarboxylase immunoreactive neurons and axons in the rat medial geniculate body. J Comp Neurol 278:47–68. CrossRef Medline

Winer JA, Larue DT (1996) Evolution of GABAergic circuitry in the mam-

malian medial geniculate body. Proc Natl Acad Sci U S A 93:3083–3087. CrossRef Medline

Winer JA, Saint Marie RL, Larue DT, Oliver DL (1996) GABAergic feedforward projections from the inferior colliculus to the medial geniculate body. Proc Natl Acad Sci U S A 93:8005–8010. CrossRef Medline

Winer JA, Larue DT, Huang CL (1999) Two systems of giant axon terminals in the cat medial geniculate body: convergence of cortical and GABAergic inputs. J Comp Neurol 413:181–197. CrossRef Medline

Wisden W, Laurie DJ, Monyer H, Seeburg PH (1992) The distribution of 13 GABAA receptor subunit mRNAs in the rat brain. I. Telencephalon, diencephalon, mesencephalon. J Neurosci 12:1040–1062. Medline

Yang S, Weiner BD, Zhang LS, Cho SJ, Bao S (2011) Homeostatic plasticity drives tinnitus perception in an animal model. Proc Natl Acad Sci U S A 108:14974–14979. CrossRef Medline

Yu XJ, Xu XX, He S, He J (2009) Change detection by thalamic reticular neurons. Nat Neurosci 12:1165–1170. CrossRef Medline